TECHNICAL NOTE

D-892

LOW-SUBSONIC MEASUREMENTS OF THE STATIC STABILITY AND

CONTROL AND OSCILLATORY STABILITY DERIVATIVES OF A

PROPOSED REENTRY VEHICLE HAVING AN EXTENSIBLE

HEAT SHIELD FOR HIGH-DRAG REENTRY

By Joseph L. Johnson, Jr., and Peter C. Boisseau

Langley Research Center
Langley Field, Va.
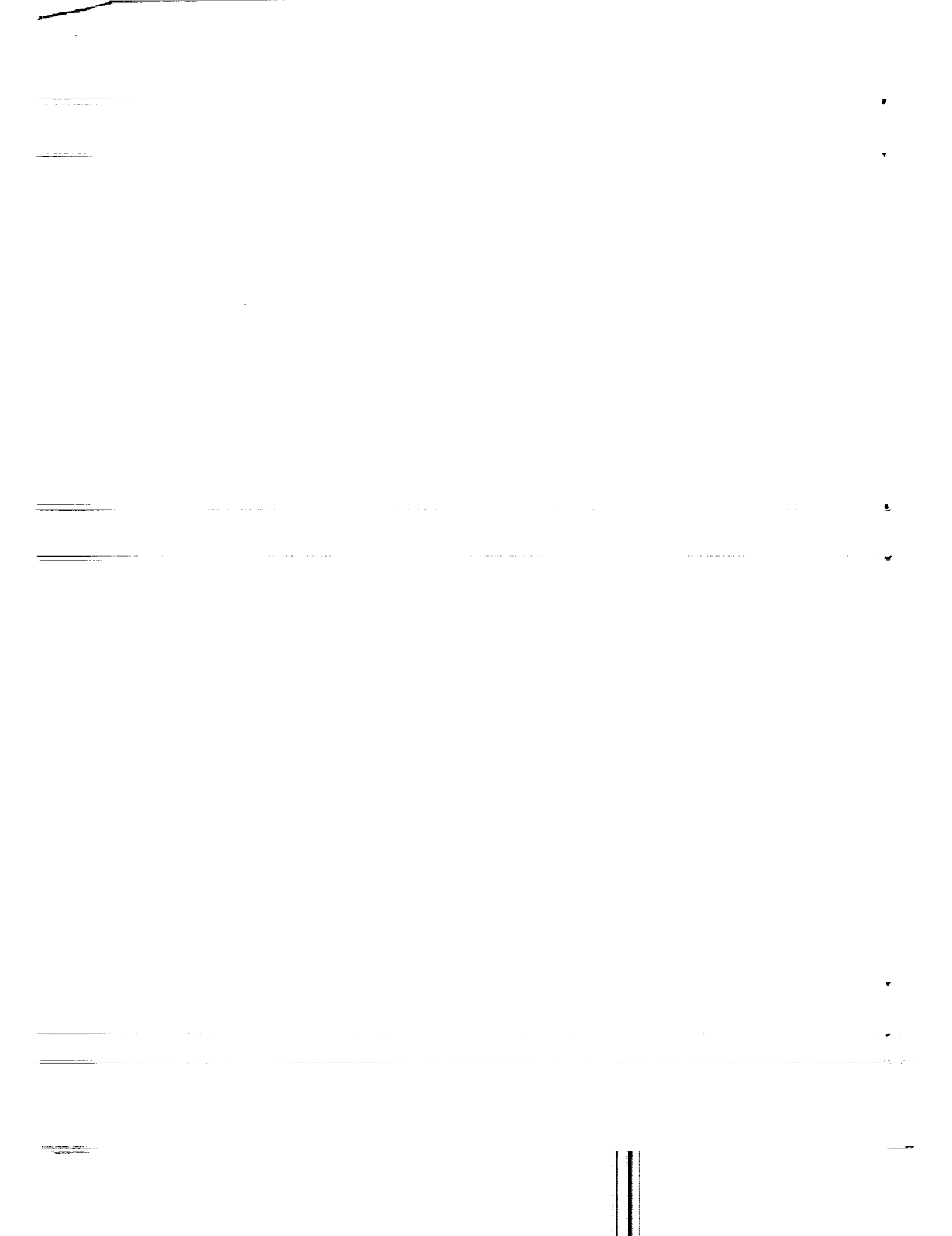
NATIONAL AERONAUTICS AND SPACE ADMINISTRATION

TECHNICAL NOTE D-892

LOW-SUBSONIC MEASUREMENTS OF THE STATIC STABILITY AND

CONTROL AND OSCILLATORY STABILITY DERIVATIVES OF A

PROPOSED REENTRY VEHICLE HAVING AN EXTENSIBLE

HEAT SHIELD FOR HIGH-DRAG REENTRY

By Joseph L. Johnson, Jr., and Peter C. Boisseau

L
1
3
2
9

SUMMARY

A low-speed investigation has been made to determine the static
and oscillatory longitudinal and lateral stability derivatives of a
proposed reentry vehicle having an extensible heat shield for reentry
at high angles of attack. The heat shield is extended forward to give
the desired aerodynamic-center position for high-angle-of-attack reentry
and, after completion of the reentry phase, is retracted to give sta-
bility and trim for gliding flight at low angles of attack.

Near an angle of attack of 90° the reentry configuration was stat-
ically stable both longitudinally and directionally, had positive dihe-
dral effect, and had positive damping in roll but zero damping in yaw.
The landing configuration had positive damping in pitch, roll, and yaw
over the test angle-of-attack range but was directionally unstable and
had negative dihedral effect between an angle of attack of about 10°
and 20°.

INTRODUCTION

The National Aeronautics and Space Administration is conducting a
general investigation to provide some basic information on configurations
designed for controlled reentry into the earth's atmosphere. (For example,
see refs. 1 to 3.) As part of this general study, a low-speed investi-
gation has been conducted on a model of a proposed reentry vehicle having
an extensible heat shield to provide trim for reentry at high angles of
attack. The model used in the present investigation was essentially a
very thick all-wing configuration with twin, all-movable tail surfaces.
These surfaces were located near the trailing edge of the wing and were
canted outward 45°. In the proposed vehicle, the heat shield is extended

forward to give the desired aerodynamic-center position for high-angle-of-attack reentry and, after completion of the reentry phase, is retracted to give stability and trim for gliding flight at low angles of attack. The present investigation was made to determine the low-subsonic static and oscillatory stability characteristics of the model.

The investigation included static and dynamic force tests over an angle-of-attack range from 0° to 90° for the model with the heat shield retracted and with the heat shield in several extended positions.

SYMBOLS

All velocities, forces, and moments with the exception of lift and drag were determined with respect to the body-axis system originating at the reference center-of-gravity position. (See figs. 1 and 2.) The stability derivatives and coefficients of each configuration tested were based on the area and mean aerodynamic chord of that particular configuration.

X,Y,Z longitudinal, lateral, and vertical body axes, respectively

S wing area, sq ft

b wing span, ft

$\bar{c}$ mean aerodynamic chord, ft

V free-stream velocity, fps

q_∞ free-stream dynamic pressure, lb/sq ft

f circular frequency, cps

ω angular velocity, $2\pi f$, radians/sec

k reduced-frequency parameter, $\dfrac{\omega b}{2V}$ or $\dfrac{\omega \bar{c}}{2V}$

α angle of attack, deg

β angle of sideslip, deg or radians

ϕ angle of roll, radians

ψ angle of yaw, radians

$\dot{\alpha}$ rate of change of angle of attack, radians/sec

$\dot{\beta}$ rate of change of sideslip angle, radians/sec

i_t tail incidence, deg

p rolling velocity, radians/sec

q pitching velocity, radians/sec

r yawing velocity, radians/sec

$\dot{p} = \dfrac{dp}{dt}$, radians/sec^2

$\dot{q} = \dfrac{dq}{dt}$, radians/sec^2

$\dot{r} = \dfrac{dr}{dt}$, radians/sec^2

F_L lift force, lb

F_D drag force, lb

F_A axial force, lb

F_Y side force, lb

F_N normal force, lb

L/D lift-drag ratio

M_X rolling moment, ft-lb

M_Y pitching moment, ft-lb

M_Z yawing moment, ft-lb

C_A axial-force coefficient, $F_A/q_\infty S$

C_Y lateral-force coefficient, $F_Y/q_\infty S$

C_N normal-force coefficient, $F_N/q_\infty S$

C_L lift coefficient, $F_L/q_\infty S$

C_D drag coefficient, $F_D/q_\infty S$

C_l rolling-moment coefficient, $M_X/q_\infty Sb$

C_m pitching-moment coefficient, $M_Y/q_\infty S\bar{c}$

C_n yawing-moment coefficient, $M_Z/q_\infty Sb$

$$C_{N_\alpha} = \frac{\partial C_N}{\partial \alpha} \qquad C_{N_{\dot\alpha}} = \frac{\partial C_N}{\partial\left(\frac{\dot\alpha\bar{c}}{2V}\right)} \qquad C_{N_q} = \frac{\partial C_N}{\partial\left(\frac{q\bar{c}}{2V}\right)} \qquad C_{N_{\dot q}} = \frac{\partial C_N}{\partial\left(\frac{\dot q\bar{c}^2}{4V^2}\right)}$$

$$C_{A_\alpha} = \frac{\partial C_A}{\partial \alpha} \qquad C_{A_{\dot\alpha}} = \frac{\partial C_A}{\partial\left(\frac{\dot\alpha\bar{c}}{2V}\right)} \qquad C_{A_q} = \frac{\partial C_A}{\partial\left(\frac{q\bar{c}}{2V}\right)} \qquad C_{A_{\dot q}} = \frac{\partial C_A}{\partial\left(\frac{\dot q\bar{c}^2}{4V^2}\right)}$$

$$C_{m_\alpha} = \frac{\partial C_m}{\partial \alpha} \qquad C_{m_{\dot\alpha}} = \frac{\partial C_m}{\partial\left(\frac{\dot\alpha\bar{c}}{2V}\right)} \qquad C_{m_q} = \frac{\partial C_m}{\partial\left(\frac{q\bar{c}}{2V}\right)} \qquad C_{m_{\dot q}} = \frac{\partial C_m}{\partial\left(\frac{\dot q\bar{c}^2}{4V^2}\right)}$$

$$C_{l_\beta} = \frac{\partial C_l}{\partial \beta} \qquad\qquad C_{l_r} = \frac{\partial C_l}{\partial\left(\frac{rb}{2V}\right)} \qquad\qquad C_{l_p} = \frac{\partial C_l}{\partial\left(\frac{pb}{2V}\right)}$$

$$C_{n_\beta} = \frac{\partial C_n}{\partial \beta} \qquad\qquad C_{n_r} = \frac{\partial C_n}{\partial\left(\frac{rb}{2V}\right)} \qquad\qquad C_{n_p} = \frac{\partial C_n}{\partial\left(\frac{pb}{2V}\right)}$$

$$C_{Y_\beta} = \frac{\partial C_Y}{\partial \beta} \qquad\qquad C_{Y_r} = \frac{\partial C_Y}{\partial\left(\frac{rb}{2V}\right)} \qquad\qquad C_{Y_p} = \frac{\partial C_Y}{\partial\left(\frac{pb}{2V}\right)}$$

$$C_{l_{\dot\beta}} = \frac{\partial C_l}{\partial\left(\frac{\dot\beta b}{2V}\right)} \qquad\qquad C_{l_{\dot r}} = \frac{\partial C_l}{\partial\left(\frac{\dot r b^2}{4V^2}\right)} \qquad\qquad C_{l_{\dot p}} = \frac{\partial C_l}{\partial\left(\frac{\dot p b^2}{4V^2}\right)}$$

$$C_{n_{\dot{\beta}}} = \frac{\partial C_n}{\partial\left(\frac{\dot{\beta}b}{2V}\right)} \qquad C_{n_{\dot{r}}} = \frac{\partial C_n}{\partial\left(\frac{\dot{r}b^2}{4V^2}\right)} \qquad C_{n_{\dot{p}}} = \frac{\partial C_n}{\partial\left(\frac{\dot{p}b^2}{4V^2}\right)}$$

$$C_{Y_{\dot{\beta}}} = \frac{\partial C_Y}{\partial\left(\frac{\dot{\beta}b}{2V}\right)} \qquad C_{Y_{\dot{r}}} = \frac{\partial C_Y}{\partial\left(\frac{\dot{r}b^2}{4V^2}\right)} \qquad C_{Y_{\dot{p}}} = \frac{\partial C_Y}{\partial\left(\frac{\dot{p}b^2}{4V^2}\right)}$$

In the present investigation the term "in-phase derivative" refers to any one of the oscillatory derivatives that are based on the components of forces and moments in phase with the angle of pitch, roll, or yaw produced in the oscillatory tests. The term "out-of-phase derivative" refers to any one of the stability derivatives that are based on the components of forces and moments 90° out of phase with the angle of pitch, roll, or yaw. The oscillatory derivatives of the present investigation were measured in the following combinations:

$$\left.\begin{array}{c} C_{m_\alpha} - k^2 C_{m_{\dot{q}}} \\[2ex] C_{A_\alpha} - k^2 C_{A_{\dot{q}}} \\[2ex] C_{N_\alpha} - k^2 C_{N_{\dot{q}}} \end{array}\right\} \quad \text{In-phase pitching derivatives}$$

$$\left.\begin{array}{c} C_{m_q} + C_{m_{\dot{\alpha}}} \\[2ex] C_{A_q} + C_{A_{\dot{\alpha}}} \\[2ex] C_{N_q} + C_{N_{\dot{\alpha}}} \end{array}\right\} \quad \text{Out-of-phase pitching derivatives}$$

$$\left.\begin{array}{c} C_{l_\beta} \sin \alpha - k^2 C_{l_{\dot{p}}} \\[2ex] C_{n_\beta} \sin \alpha - k^2 C_{n_{\dot{p}}} \\[2ex] C_{Y_\beta} \sin \alpha - k^2 C_{Y_{\dot{p}}} \end{array}\right\} \quad \text{In-phase rolling derivatives}$$

$$C_{l_p} + C_{l_{\dot\beta}} \sin \alpha$$

$$C_{n_p} + C_{n_{\dot\beta}} \sin \alpha$$

$$C_{Y_p} + C_{Y_{\dot\beta}} \sin \alpha$$

$\left.\right\}$ Out-of-phase rolling derivatives

$$C_{l_\beta} \cos \alpha + k^2 C_{l_{\dot r}}$$

$$C_{n_\beta} \cos \alpha + k^2 C_{n_{\dot r}}$$

$$C_{Y_\beta} \cos \alpha + k^2 C_{Y_{\dot r}}$$

$\left.\right\}$ In-phase yawing derivatives

$$C_{l_r} - C_{l_{\dot\beta}} \cos \alpha$$

$$C_{n_r} - C_{n_{\dot\beta}} \cos \alpha$$

$$C_{Y_r} - C_{Y_{\dot\beta}} \cos \alpha$$

$\left.\right\}$ Out-of-phase yawing derivatives

MODEL AND APPARATUS

The investigation was made with a model of a proposed reentry vehicle having an extensible heat shield for reentry at high angles of attack. The heat shield is extended forward to give the desired aerodynamic-center position for high angle-of-attack reentry and is retracted to give stability and trim for gliding flight at low angles of attack. The proposed configuration has twin, all-movable tail surfaces which are retracted for reentry and canted outward 45° for gliding flight. In the model, no provision was made for retracting or extending the heat shield or tail surfaces. The extensible heat shield feature was simulated by the use of four different size heat shields which varied in length from the retracted case (heat shield 1) to the fully extended case (heat shield 4) and included two intermediate positions (heat shields 2 and 3). The tails were mounted for easy removal to facilitate testing of these configurations with tails off and on.

For all the heat shield configurations tested, the reference center of gravity was held fixed at one position relative to the stationary part of the wing. With the heat shield retracted (landing configuration), this fixed center-of-gravity position corresponded to 25 percent of the root chord of heat shield 1. As the heat shield was extended, the center-of-gravity position in percentage of root chord corresponded to a more rearward location until, with the heat shield fully extended (reentry configuration), the model had a design center-of-gravity position of 50 percent of the root chord of heat shield 4. The dimensional characteristics of the model in the various configurations tested are given in table I and a three-view drawing of the model is presented in figure 2.

In all force tests, a sting-type support system and a strain-gage balance were used. A photograph of the static-force-test setup with the model mounted for testing is shown in figure 3. The rotary oscillation tests were made on an oscillation apparatus in which the model was oscillated in either pitch, roll, or yaw. Sketches of this apparatus with the model mounted for rolling and yawing tests are shown in figure 4. For the pitching tests, the apparatus was similar to that for the yawing tests except that the model was mounted from the side with the sting coincident with the Y body axis.

In the oscillation test apparatus, electrical resolvers were geared directly to the drive-shaft mechanism to generate electrical signals proportional to the displacement and velocity of the model. This resolver system permitted a direct reading of the balance output signals either in-phase with or out-of-phase with angular displacement of the model by means of manually operated, null-seeking, read-out equipment. A complete description of this apparatus and instrumentation is presented in reference 4.

TESTS

Static and dynamic force tests were made over an angle-of-attack range from 0° to 90° to determine the static and oscillatory longitudinal and lateral stability characteristics of the model with the heat shield retracted and with the heat shield fully extended. In addition, static longitudinal tests were made for two intermediate positions of the heat shield. All these tests were made for the model with the tails off and on.

The static lateral stability characteristics were measured over an angle-of-sideslip range from -20° to 20°. The rotary oscillation tests were made for amplitudes of ±5° in pitch, roll, and yaw. Most of the oscillation tests were for a frequency of about 1.0 cycle per second,

which corresponds to a reduced-frequency parameter k of about 0.10. A few tests were made in which the velocity and frequency range of the tests were varied.

Most of the tests were made at a dynamic pressure of 4.1 pounds per square foot, which corresponds to an airspeed of about 60 feet per second. Some of the oscillation tests were made at a dynamic pressure of 1.6 pounds per square foot, which corresponds to an airspeed of about 37 feet per second. The Reynolds number range covered in these tests varied from about 503,000 to 1,240,000 based on the mean aerodynamic chords of the wings (heat shields) investigated.

RESULTS AND DISCUSSION

Static-Force-Tests Results

Longitudinal characteristics.- The static longitudinal stability and control data for the various configurations tested are presented in figure 5. The data of figure 5(a) show that the model was statically stable and trimmed in pitch at an angle of attack of about 78° with tails off and with the heat shield fully extended (reentry configuration). This configuration was statically unstable at low angles of attack since the center of gravity was positioned at 50 percent of the root chord. Simulating the retraction of the heat shield, by progressively reducing its size, reduced the instability of the model at low angles of attack and moved the stable trim point from about 78° for the heat shield fully extended case to about 18° for the heat shield fully retracted case (landing configuration). The landing configuration was still statically unstable, however, at lower angles of attack.

The addition of the tails to the model (compare figs. 5(a) and 5(b)) had little effect on the stability of the reentry configuration but, as the size of the heat shield was decreased, the pitching-moment contribution of the tails in the lower angle-of-attack range increased. For the landing configuration, the addition of the tails resulted in the model being statically stable at low angles of attack although an unstable break occurred in the pitching-moment curve between an angle of attack of 10° and 15°.

The results of tests to determine the effect on the longitudinal characteristics of deflecting the all-movable surfaces as elevators (fig. 5(c)) indicate that the instability between an angle of attack of 10° and 15° can be attributed to tail stall since deflection of the surfaces to negative angles of incidence delayed the unstable break in the pitching-moment curve to higher angles of attack. This early stall

of the tails (for the 0° incidence condition) can probably be attributed to a strong upwash flow field near the tail locations which was induced by the wing tip vortices. With a tail incidence of -15°, the model was statically stable and trimmed in pitch at an angle of attack of about 8° with a maximum value of trimmed lift-drag ratio of about 5.3.

Lateral characteristics. - The static lateral stability coefficients for the tails off and on conditions are plotted against angle of sideslip in figures 6 and 7 for the reentry and landing configurations, respectively. The data are generally linear for small sideslip angles except for the landing configuration at an angle of attack of 40° with the tails off (fig. 7(a)) and between angles of attack of 10° and 30° with the tails on (fig. 7(b)). The lateral stability parameters C_{Y_β}, C_{n_β}, and C_{l_β} determined for angles of sideslip of $\pm 5^\circ$ from figures 6 and 7 are presented in figure 8 as a function of angle of attack.

The data of figure 8 show that the reentry configuration with tails off was about neutrally or very slightly directionally stable from an angle of attack of about 50° to 90°. The effective dihedral for this configuration was positive $\left(-C_{l_\beta}\right)$ over the test angle-of-attack range. The addition of the tails to this configuration contributed an increment of directional stability and positive dihedral effect which generally decreased with increasing angle of attack and became relatively small at an angle of attack of 90°.

The lateral characteristics for the landing configuration with tails off are generally similar to those of the tail-off reentry configuration. The lateral stability parameters for the landing configuration were omitted from this plot between angles of attack of 30° and 50° because of erratic variations of the lateral coefficients with sideslip angle for an angle of attack of 40°. (See fig. 7(a).) This erratic variation in the forces and moments of the tail-off landing condition is difficult to explain since it did not occur for the tail-on landing condition or for the reentry condition with tails off or on. It is apparently associated with intermittent stall effects which introduced large asymmetrical flow conditions over the model near maximum lift.

In the case of the landing configuration with tails on, the directional stability and effective dihedral were positive at an angle of attack of 0° but both of these factors decreased rapidly and became negative in the angle-of-attack range of most interest for landing (between 10° and 20°). These effects are probably a result of unfavorable flow conditions at the tails which resulted in the tails becoming destabilizing. The unfavorable flow conditions on the tails are probably associated with some asymmetry in the vortex flow at the rear of the

model produced by sideslip. (From past experience it has been found that configurations having negative directional stability and negative dihedral effect are likely to have unsatisfactory lateral flight characteristics.)

The effectiveness of the all-movable tail surfaces as lateral control is shown in figure 9 for the model in the landing configuration. The data show that differential deflection of these surfaces to produce positive yawing moments also produced large negative rolling moments at an angle of attack of 0°. These adverse rolling moments decreased rapidly to zero with increasing angle of attack while the yawing moments remained fairly large up to an angle of attack of about 35°. The ratio of yawing moment to rolling moment produced by differential control deflection in this case can be related directly to the dihedral angle of the tails. In tail arrangements having positive dihedral, differential deflection of the control surfaces to produce positive yawing moments results in a positive angle of attack on the right surface and a negative angle of attack on the left surface. This relationship introduces increments of positive and negative lift on the right and left surfaces, respectively, which combine to produce large adverse rolling moments. Increasing the angle of attack of the model reduces and eventually reverses these lift increments because the right surface stalls and becomes ineffective while the angle of attack of the left surface changes from negative to positive. Such an effect probably would account for the rapid decrease in the adverse rolling moments of the tails of the model with increasing angle of attack. It is also possible that this variation in the tail rolling moment with angle of attack could be greatly influenced by loads induced on the wing of the model by differential control deflection.

In connection with the preceding discussion, it is of interest to point out that some of the effects associated with differential control deflection might introduce changes in longitudinal stability and trim characteristics of the model. No tests of this nature were made in this investigation but it is possible that such effects might be great enough in this particular case to warrant consideration.

L
1
3
2
9

Longitudinal Oscillatory Derivatives

In-phase derivatives.- The longitudinal oscillatory derivatives obtained in phase with angular displacement during pitching oscillation tests of the model in the reentry and landing configurations are presented in figure 10(a). Also presented in this figure for the purpose of comparison are static values (k = 0) of the longitudinal stability parameters taken from figure 5. In general, the static and oscillatory data show similar trends with angle of attack although there are some

large differences in the data in some instances for both the reentry and landing configuration. It is believed that the $k^2C_{m_{\dot{q}}}$, $k^2C_{A_{\dot{q}}}$, and $k^2C_{N_{\dot{q}}}$ components of the in-phase derivatives are generally relatively small and that most of the large differences in the data can be attributed to the effects of frequency on the C_{m_α}, C_{A_α}, and C_{N_α} components of the derivatives. Other studies have shown this effect to be large in cases where considerable flow separation was present. (See refs. 4 and 5.)

Out-of-phase derivatives.- Values of the out-of-phase oscillatory derivatives measured in the pitching oscillation tests of the model in the reentry and landing configurations are presented in figure 10(b). The data show that the model in the reentry configuration with tails off or on generally had a slight amount of positive damping in pitch over the test angle-of-attack range except from an angle of attack of about 20° to 50° where the model had large positive values of $C_{m_q} + C_{m_{\dot\alpha}}$ (negative damping). Large positive values of $C_{N_q} + C_{N_{\dot\alpha}}$ were measured in about the same angle-of-attack range where maximum negative damping occurred. The negative damping in pitch for the reentry configuration between an angle of attack of 20° and 50° may not be of great significance in this case since in this intermediate angle-of-attack range the heat shield would be partly retracted during transition from reentry to gliding flight. The configuration with the intermediate heat-shield position would have damping characteristics somewhere between those of the reentry and landing configurations. There is one point of interest in this connection, however, which should be mentioned. Analysis based on two-degree-of-freedom longitudinal stability equations indicates that the model in the reentry configuration would be dynamically longitudinally unstable at an angle of attack of 90° (despite positive values of damping in pitch) because of the destabilizing effect of the negative lift-curve slope of this configuration at this angle of attack. (See fig. 5.) If the amplitudes of the unstable oscillation in this case were allowed to build up to values which corresponded to the angle-of-attack region where negative damping occurred, then the instability of the configuration would be aggravated and a more violent divergence would occur. Unpublished results of dynamic tests made in the Langley 20-foot free-spinning tunnel substantiate the results of this analysis. It was found that wings having planforms similar to that of the reentry configuration of the present investigation were dynamically unstable at an angle of attack of 90° and experienced a diverging oscillation which built up rapidly in amplitude and eventually led to a violent tumbling motion.

The large increase in magnitude of $C_{N_q} + C_{N_{\dot\alpha}}$ and $C_{m_q} + C_{m_{\dot\alpha}}$ near

an angle of attack of 40° for the reentry configuration is believed to be related to the effects of flow separation on the wing which greatly increased the $\dot\alpha$ component of the total derivatives. This effect is probably similar to that pointed out in lateral oscillation tests reported in reference 6 where the occurrence of flow separation was shown to produce incremental forces and moments which may either lag or lead the model angular motion to give large $\dot\beta$ derivatives. In pitching oscillation tests, a similar type of phenomenon probably occurs, particularly at angles of attack near maximum lift coefficient since this is the angle-of-attack region where large flow separation effects are likely to occur. On this basis, therefore, it appears that the large positive values of $C_{m_q} + C_{m_{\dot\alpha}}$ which were measured for the reentry configurations can be

related to the large positive values of $C_{N_q} + C_{N_{\dot\alpha}}$ produced by flow

separation and to an aerodynamic-center shift which lagged the angular motion of the model. In this case the center of gravity was located at the centroid of area, and the lag between the aerodynamic-center shift and model motion produced destabilizing effects (negative damping). At higher angles of attack where the wing was completely stalled this type of aerodynamic-center shift apparently did not occur and, even though fairly large values of $C_{N_{\dot\alpha}}$ are still in evidence, only small increments

of $C_{m_{\dot\alpha}}$ are realized.

The data for the landing configuration (fig. 10(b)) show negative values of $C_{m_q} + C_{m_{\dot\alpha}}$ (positive damping) over the test angle-of-attack

range with maximum values of damping occurring between an angle of attack of 40° and 60°. In this case the damping was greater than that for the reentry configuration because the center of gravity (or point of rotation) was located at the aerodynamic center rather than at the 50-percent-chord point which was aft of the aerodynamic center. The effects of flow separation for this condition appeared to be stabilizing (produced positive damping), which indicates that the phase relationship between the aerodynamic-center shift and model motion was opposite to that for the reentry configuration.

Lateral Oscillatory Derivatives

In-phase derivatives.- The lateral oscillatory derivatives obtained in phase with angular displacement during the rolling and yawing oscillation tests of the model in the landing and reentry configuration are

presented in figure 11. Also presented in this figure for purposes of comparison are static values (k = 0) of the lateral stability parameters taken from figure 8. In general, the static and oscillatory test results show similar trends with angle of attack, but the agreement appears to be a little better for the reentry configuration than for the landing configuration.

Out-of-phase rolling oscillatory derivatives.- Values of the out-of-phase oscillatory derivatives measured in the rolling oscillation tests of the model in the reentry and landing configurations are presented in figure 12. These data show that the model had positive damping in roll $\left(-\left(C_{l_p} + C_{l_{\dot{\beta}}} \sin \alpha\right)\right)$ over the test angle-of-attack range for both the reentry and landing configurations. In the low angle-of-attack range the landing configuration with tails on had relatively large values of damping because of large increments of damping contributed by the tails. It is interesting to note that the tails contributed these large increments of damping in roll in the same angle-of-attack range where statically they were found to produce large increments of negative dihedral effect. (See fig. 8.) This relationship is similar to that noted in previous studies (ref. 5) and can be attributed to a sidewash flow over the tails which decreases the tail effectiveness under static conditions but lags the model motion under dynamic conditions to increase the tail effectiveness. (In other words, a sidewash flow which decreases C_{n_β} and $-C_{l_\beta}$ of a tail will produce increments of $C_{n_{\dot{\beta}}}$ and $-C_{l_{\dot{\beta}}}$ to increase the damping contribution of the tail.)

The reentry configuration with tails off showed small values of the cross derivative $C_{n_p} + C_{n_{\dot{\beta}}} \sin \alpha$ whereas the landing configuration with tails off had relatively large negative values of this derivative at low angles of attack. The addition of the tails resulted in the reentry configuration having positive values of $C_{n_p} + C_{n_{\dot{\beta}}} \sin \alpha$ over most of the test angle-of-attack range but generally reduced the negative values of this derivative for the landing configuration at low angles of attack.

Out-of-phase yawing oscillatory derivatives.- Values of the out-of-phase oscillatory derivatives measured in yawing oscillation tests of the model in the reentry and landing configurations are presented in figure 13. The data for the reentry configuration show relatively small values of the damping-in-yaw derivative $C_{n_r} - C_{n_{\dot{\beta}}} \cos \alpha$ and of the cross derivative $C_{l_r} - C_{l_{\dot{\beta}}} \cos \alpha$. Near an angle of attack of 90°, this configuration had values of these derivatives of approximately zero.

The data for the landing configuration with tails on show large negative values of $C_{n_r} - C_{n_{\dot\beta}} \cos \alpha$ (positive damping) and large positive values of $C_{l_r} - C_{l_{\dot\beta}} \cos \alpha$ at low angles of attack. These values can be attributed almost entirely to the tail contribution to these derivatives. Here again, these large tail increments can be attributed to large values of $C_{n_{\dot\beta}}$ and $-C_{l_{\dot\beta}}$ produced by lag of sidewash effects on the tails.

SUMMARY OF RESULTS

The results of a low-speed investigation made to determine the static and oscillatory stability derivatives of a proposed reentry vehicle having an extensible heat shield for reentry at high angles of attack are summarized as follows:

1. Near an angle of attack of 90° the reentry configuration was statically stable both longitudinally and directionally, had positive dihedral effect, and had positive damping in roll but zero damping in yaw.

2. The landing configuration had positive damping in pitch, roll, and yaw over the angle-of-attack range but was directionally unstable and had negative dihedral effect between an angle of attack of about 10° and 20°.

Langley Research Center,
National Aeronautics and Space Administration,
Langley Field, Va., May 4, 1961.

REFERENCES

1. Staff of Langley Flight Research Division (Compiled by Donald C. Cheatham): A Concept of a Manned Satellite Reentry Which Is Completed With a Glide Landing. NASA TM X-226, 1959.

2. Ware, George M.: Low-Subsonic-Speed Static Longitudinal Stability and Control Characteristics of a Winged Reentry-Vehicle Configuration Having Wingtip Panels That Fold Up for High-Drag Reentry. NASA TM X-227, 1960.

3. Jackson, Charlie M., and Harris, Roy V., Jr.: Static Longitudinal Stability and Control Characteristics at a Mach Number of 1.99 of a Lenticular-Shaped Reentry Vehicle. NASA TN D-514, 1960.

4. Hewes, Donald E.: Low-Subsonic Measurements of the Static and Oscillatory Lateral Stability Derivatives of a Sweptback-Wing Airplane Configuration At Angles of Attack From -10° to 90°. NASA MEMO 5-20-59L, 1959.

5. Johnson, Joseph L., Jr.: Low-Speed Measurements of the Static and Oscillatory Lateral Stability Derivatives of a Model of a Canard Airplane Designed for Supersonic Cruise Flight. NASA TM X-15, 1959.

6. Campbell, John P., Johnson, Joseph L., Jr., and Hewes, Donald E.: Low-Speed Study of the Effect of Frequency on the Stability Derivatives of Winds Oscillating in Yaw With Particular Reference to High Angle-of-Attack Conditions. NACA RM L55H05, 1955.

TABLE I.- DIMENSIONS OF MODEL CONFIGURATIONS

	Configuration			
	Landing (Heat shield 1)	Intermediate		Reentry (Heat shield 4)
		Heat shield 2	Heat shield 3	
Heat shield:				
Area, sq ft	3.88	4.58	5.28	5.98
Span, ft	1.88	1.88	1.88	1.88
Tip chord, ft	1.68	2.06	2.43	2.80
Root chord, ft . . .	2.25	2.63	3.00	3.37
Mean aerodynamic chord, ft . . .	2.13	2.50	2.87	3.25
Aspect ratio	0.91	0.78	0.66	0.59
Center of gravity, percent $\bar{c}$	23.60	35.02	43.40	50.00
Tail surfaces:				
Area (each, to ref. line), sq ft		0.36		
Tip chord, ft		0.21		
Root chord, ft . . .		0.67		
Span (each, in plane of surface), ft		0.82		
Sweepback of L.E., deg . .		37.4		

L-1329
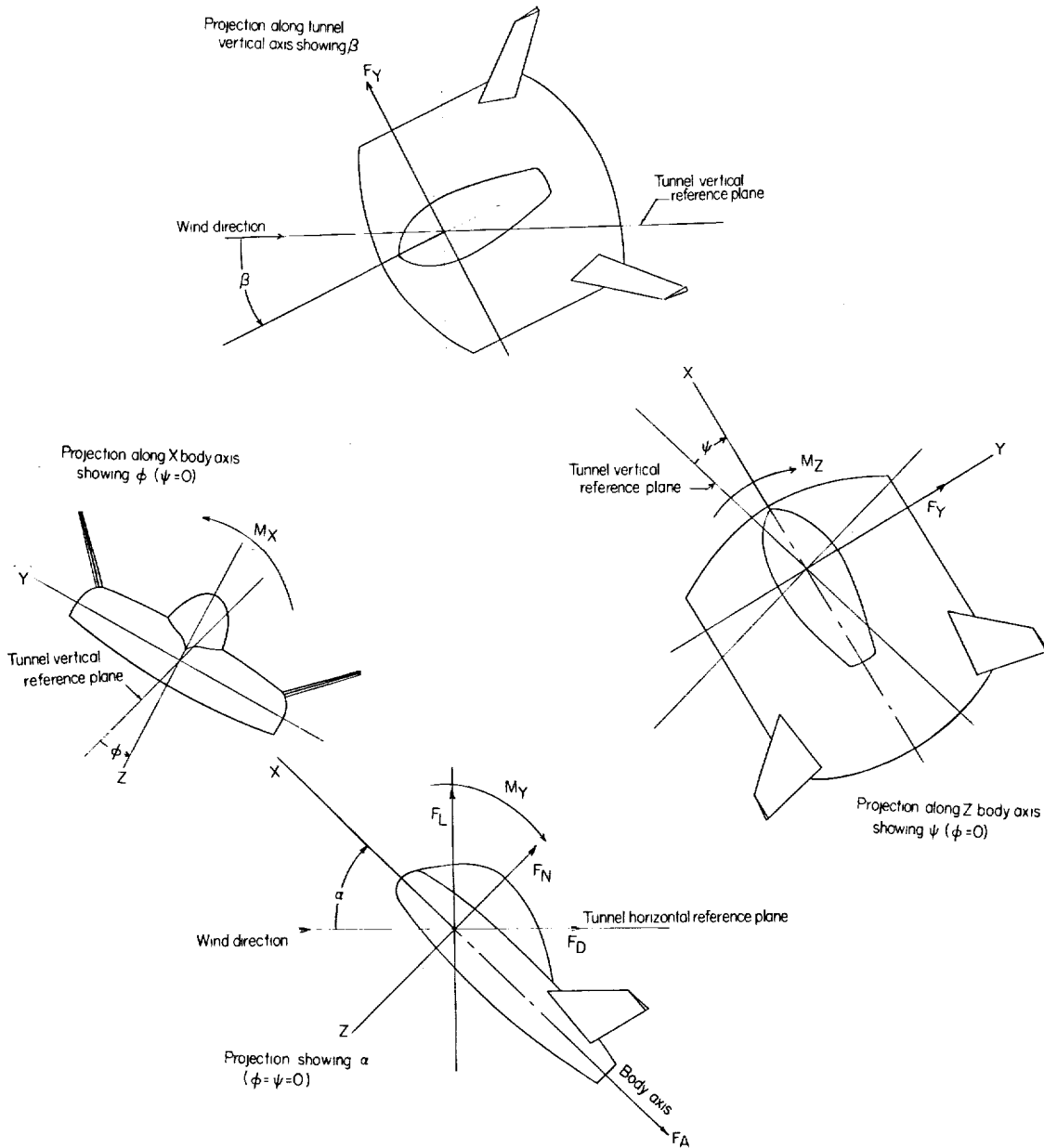
Figure 1.- The body system of axes. Arrows indicate positive direction
of moments, forces, and angles. This system of axes is defined as an
orthogonal system having the origin at the center of gravity and in
which the X-axis is in the plane of symmetry and alined with the
longitudinal axis of the fuselage, the Z-axis is in the plane of
symmetry and perpendicular to the Y-axis, and the Y-axis is perpen-
dicular to the plane of symmetry.

c.g. (landing configuration) = 0.25 root chord
(reentry configuration) = 0.50 root chord

c̄ Shield 1 = 25.54

c̄ Shield 4 = 39.00

0.73

−5.37−

−5.46−

11.25   0.75

22.50

6.72

9.87

7.0

45°

Reference line

2.75   −   8.20

Heat shield 4 = 40.50

Shield 3 = 35.96

Shield 2 = 31.52

Shield 1 = 27.00

15.88   −7.56−

6.75

1.71

8.00

.54

2.52

2.5   Reference line
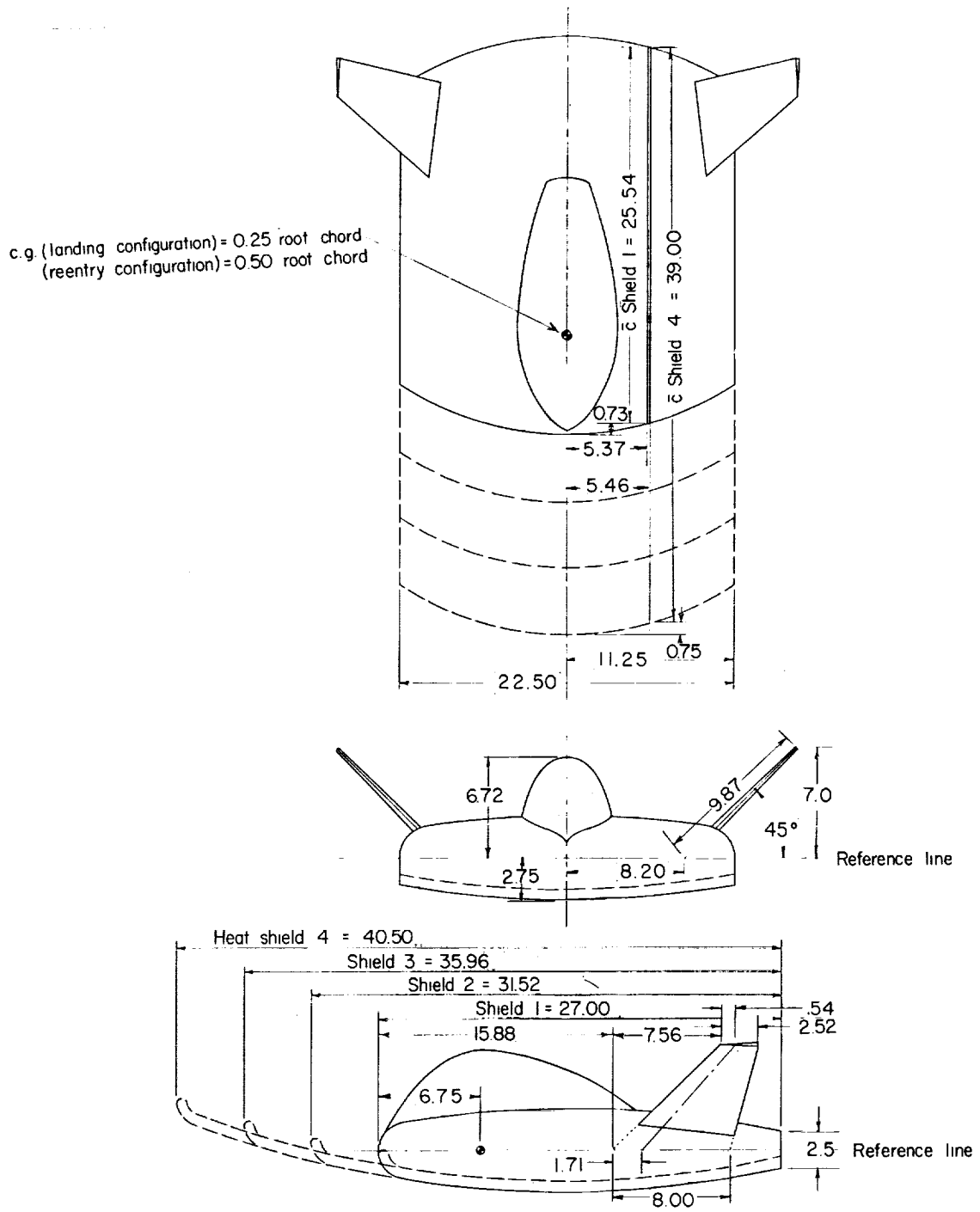
Figure 2.- Three-view drawing of the model used in the investigation.
All dimensions are in inches.

L-1329

L-59-6604

Figure 3.- Photograph of the static-force-test setup.

L-1329
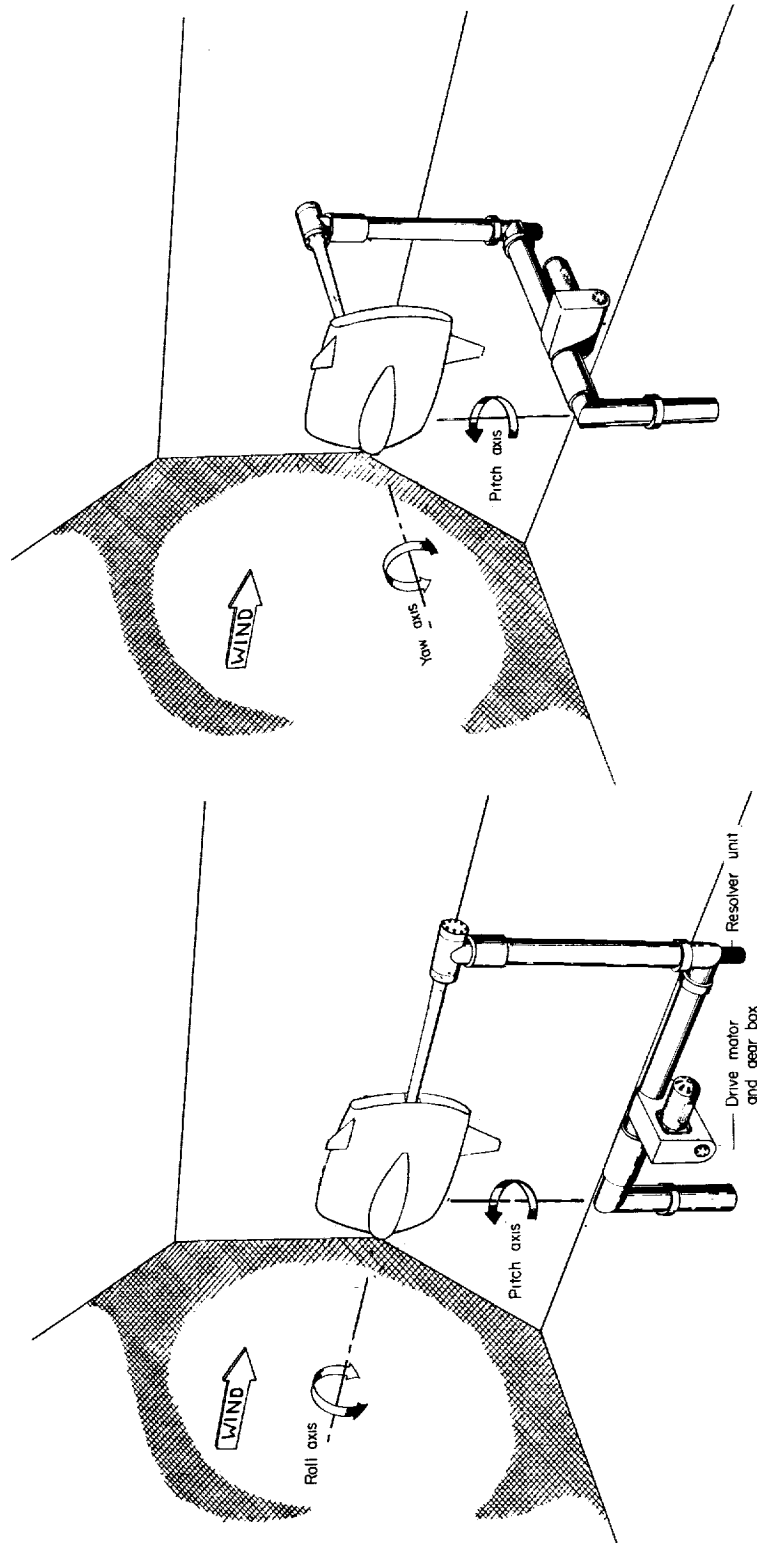
(a) Arrangement for rotary oscillation tests in roll.

(b) Arrangement for rotary oscillation tests in yaw.

Figure 4.- Schematic sketches of the oscillation test apparatus.
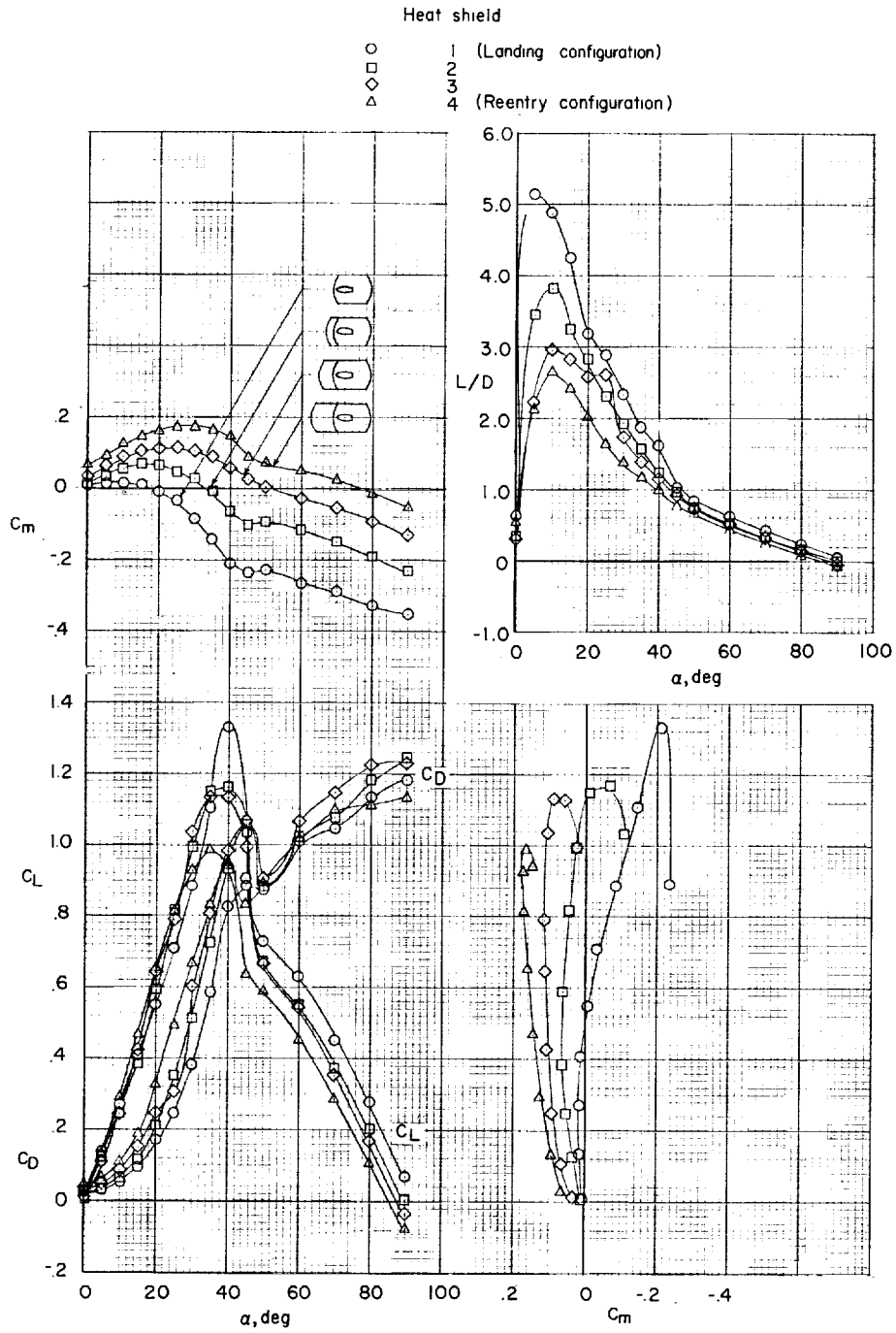
(a) Tails off.

Figure 5.- Static longitudinal stability characteristics of the model.

Heat shield

O	1	(Landing configuration)
□	2	
◇	3	
△	4	(Reentry configuration)
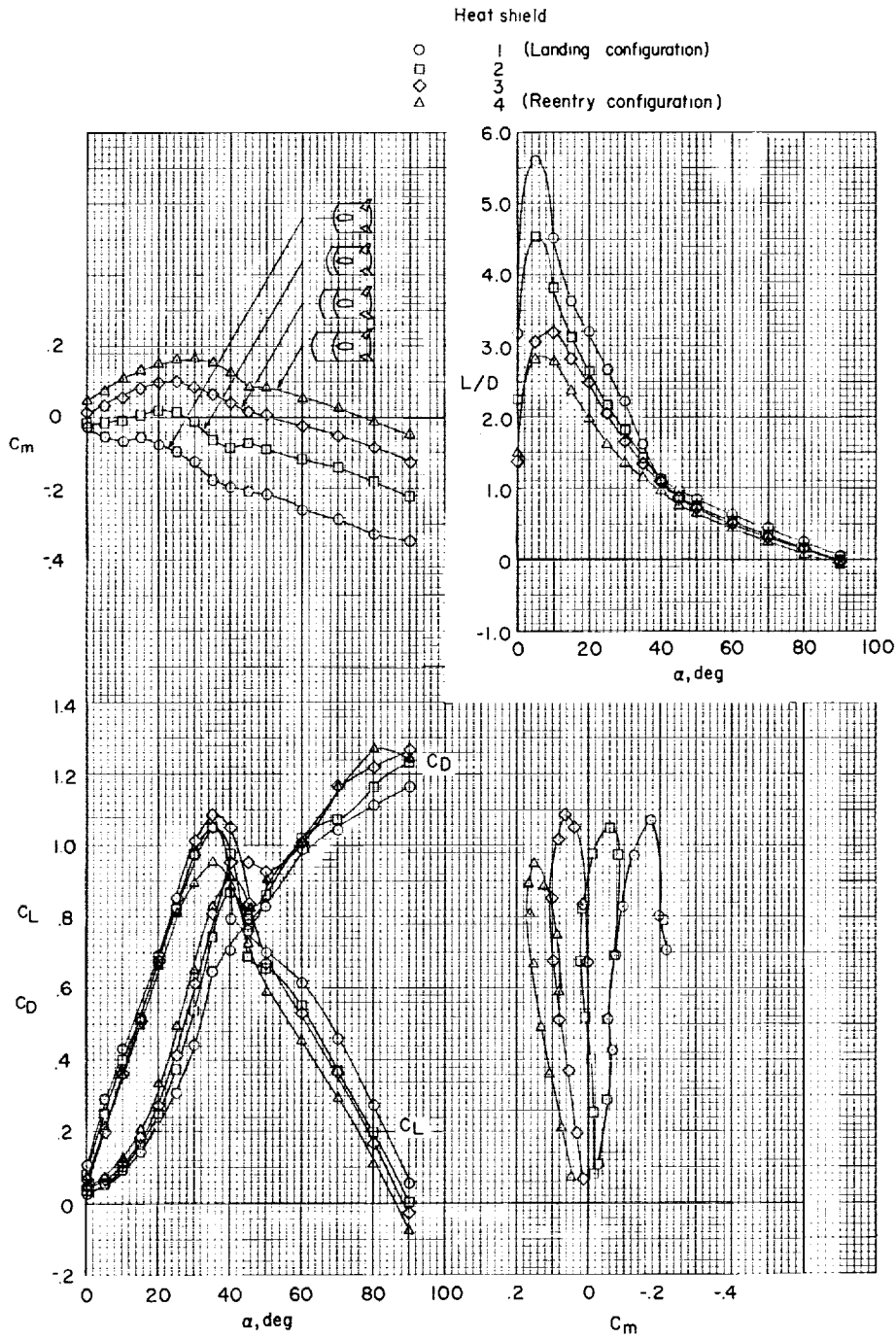
(b) Tails on.

Figure 5.- Continued.
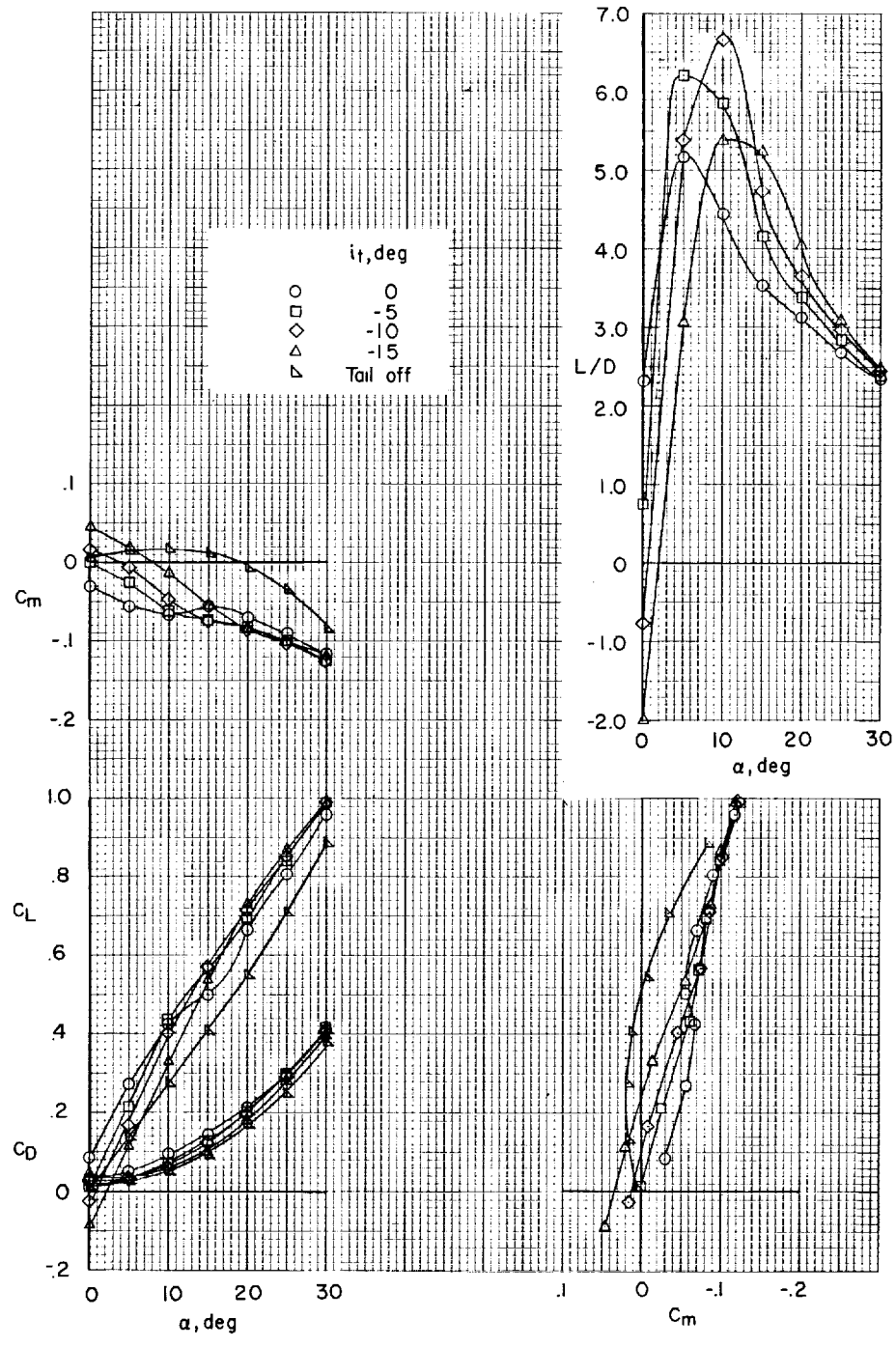
(c) Tails on; landing configuration.

Figure 5.- Concluded.
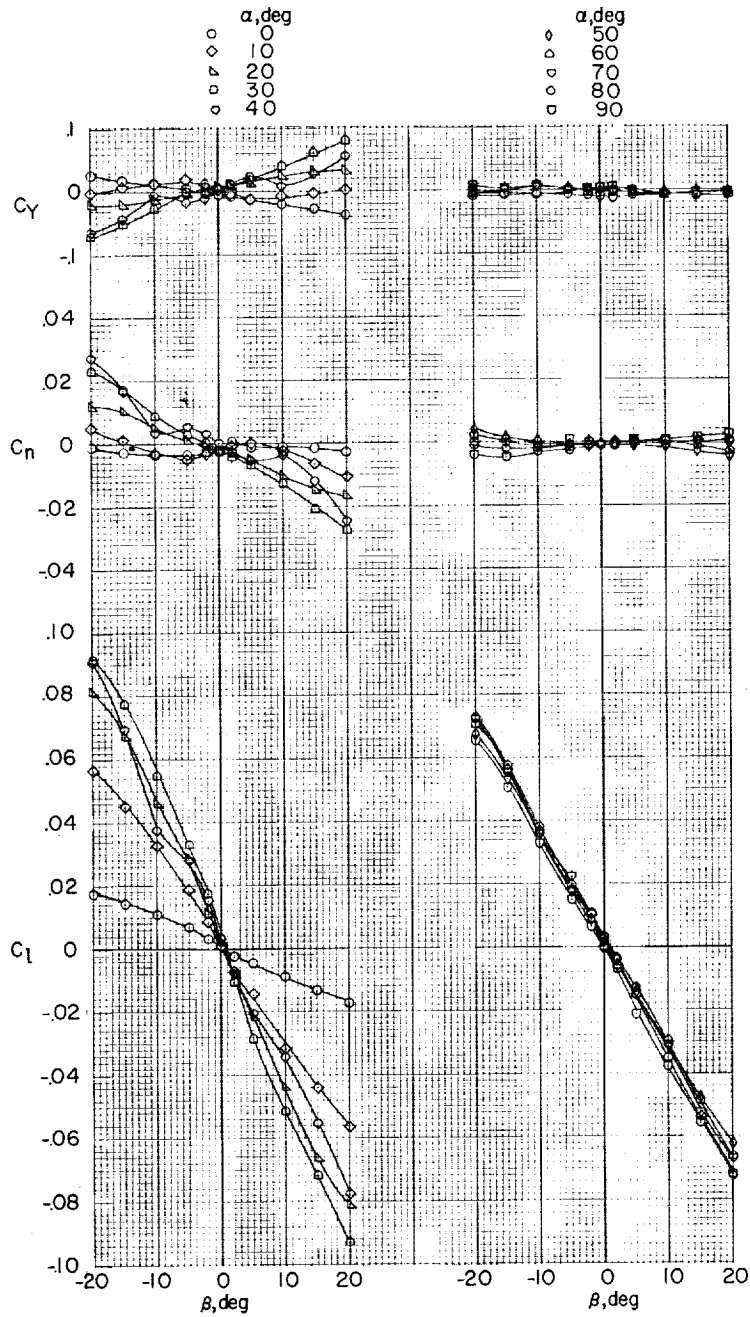
(a) Tails off.

Figure 6.- Static lateral stability characteristics of the model.
Heat shield 4 (reentry configuration).
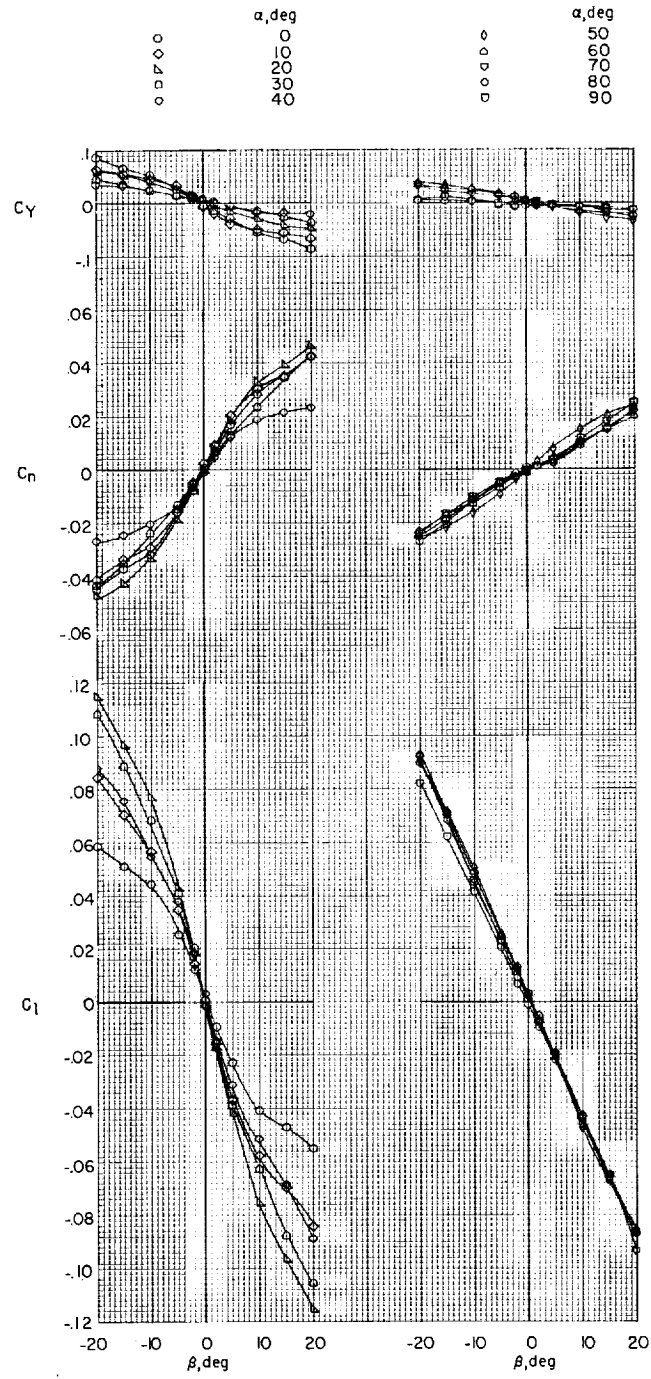
(b) Tails on.

Figure 6.- Concluded.
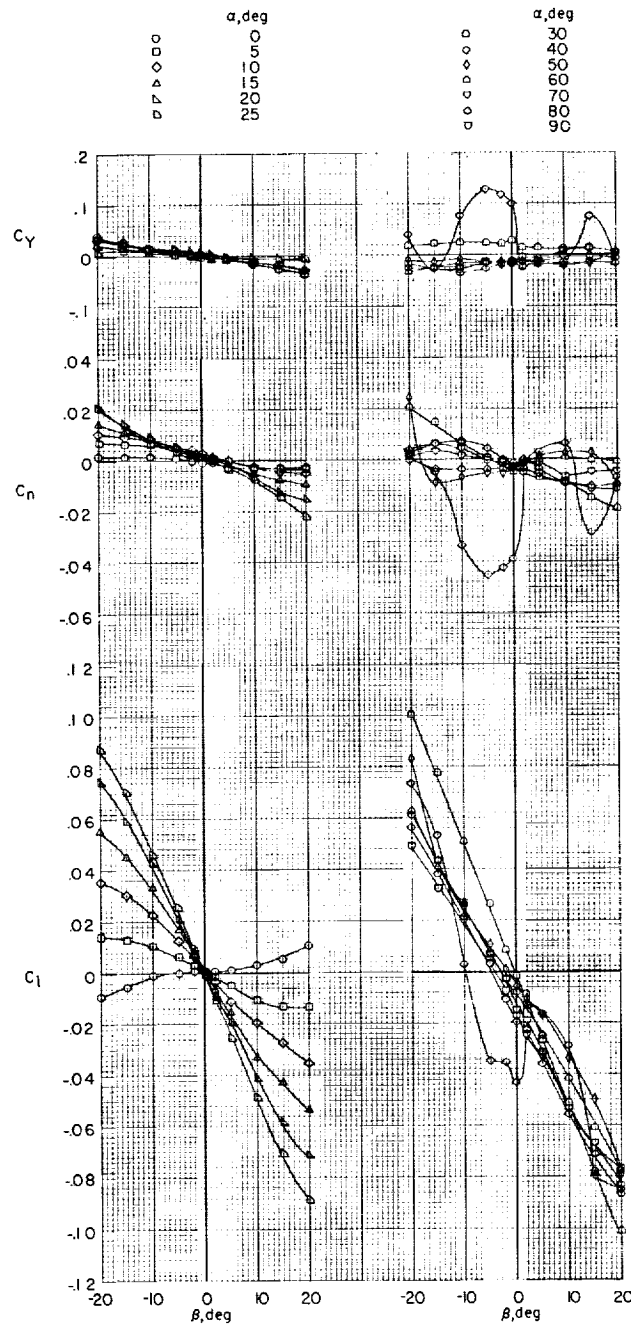
(a) Tails off.

Figure 7.- Static lateral stability characteristics of the model.
Heat shield 1 (landing configuration).

L-1329
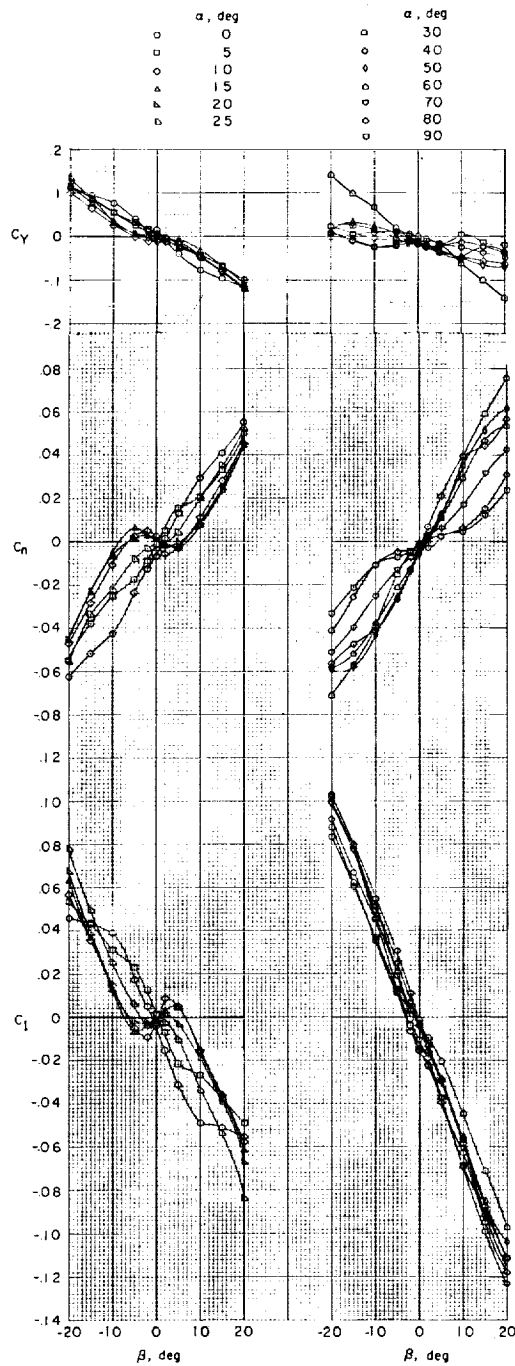
(b) Tails on.

Figure 7.- Concluded.
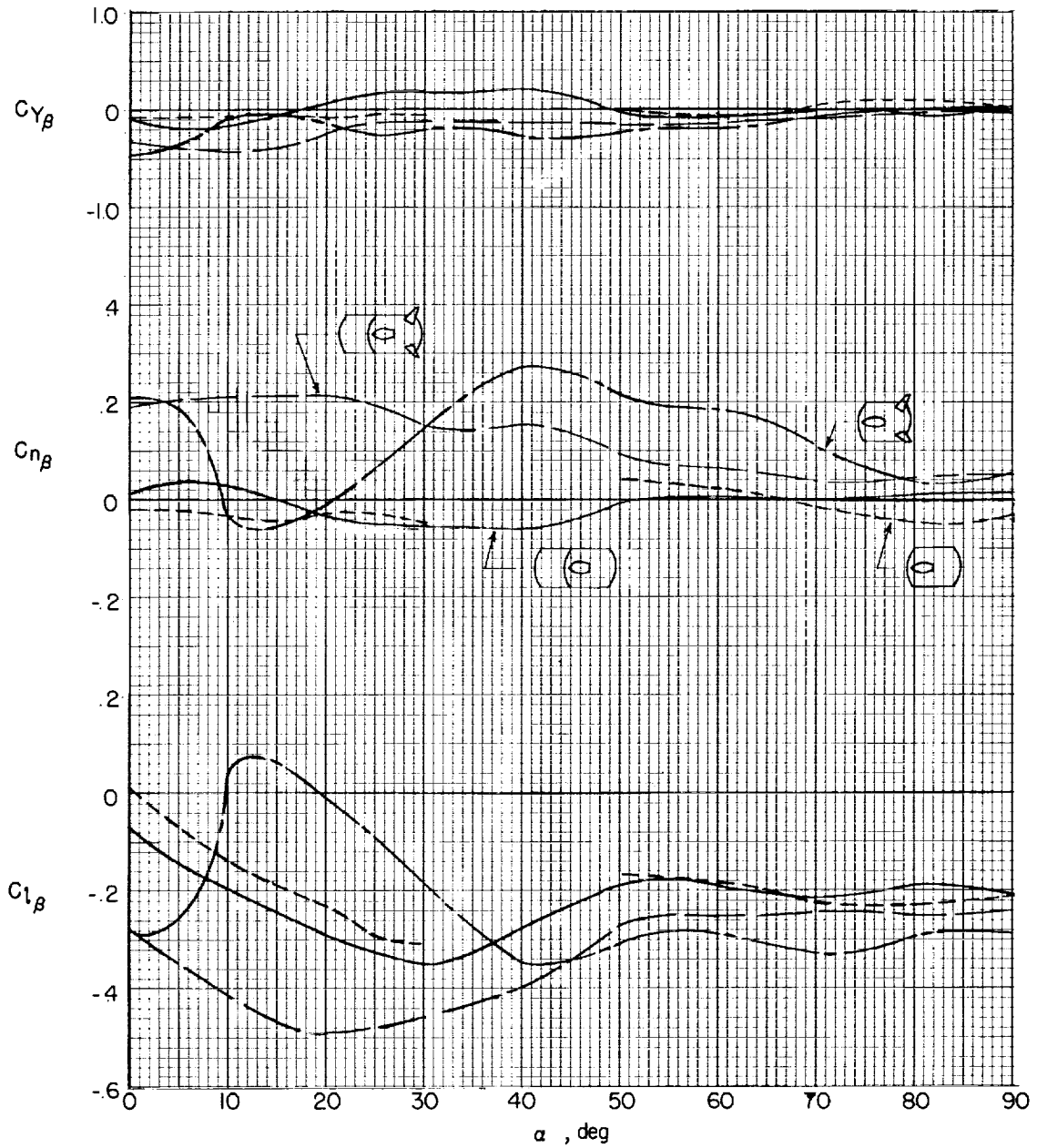
Figure 8.- Static lateral stability parameters of the model.

I-1329

Deflection of tail surfaces for
right rudder control, deg

—————— 10 (each surface)

— — — — 20 (each surface)
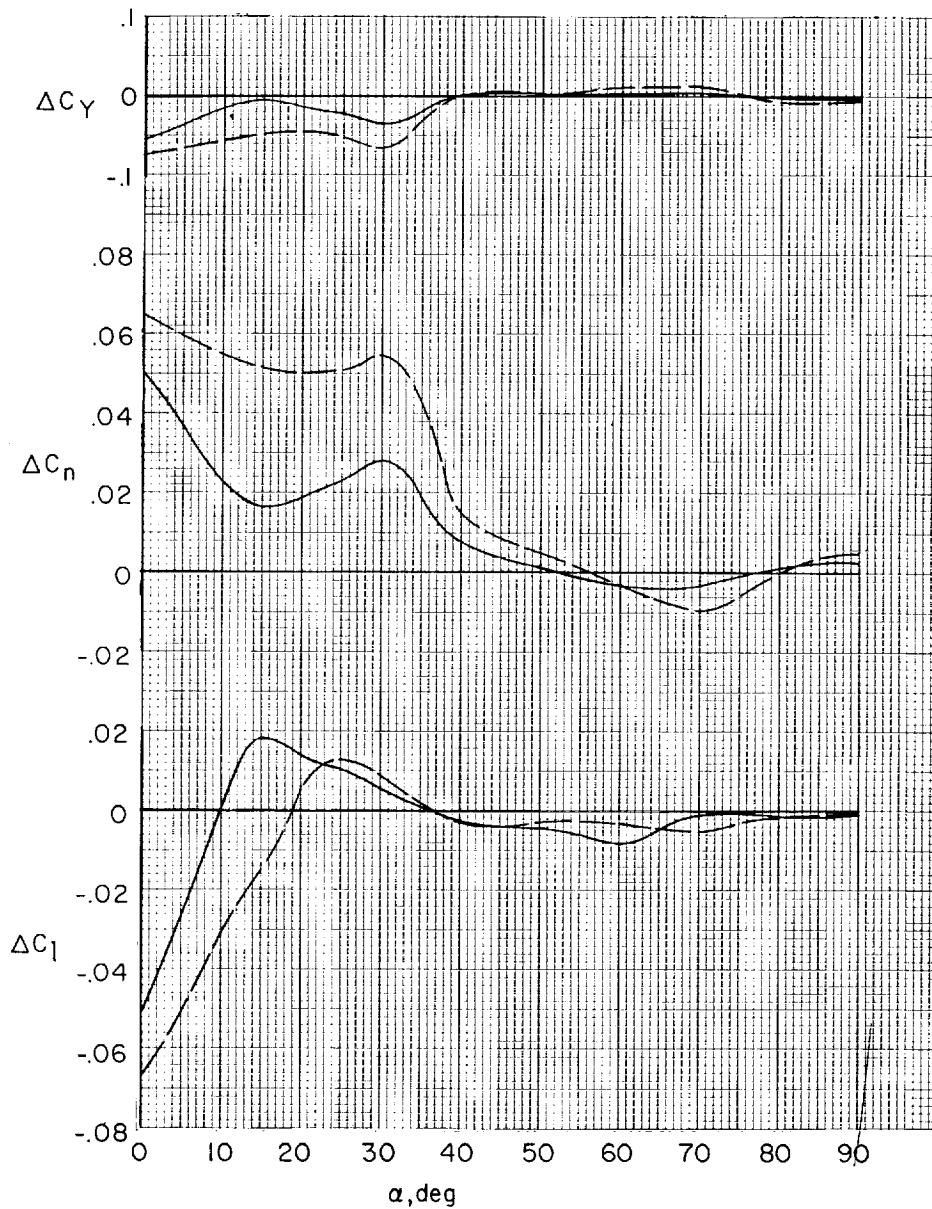
Figure 9.- Incremental lateral forces and moments produced by differ-
ential deflection of the all-movable vertical tails. Landing
configuration.

Tails   k

○   off   0.118
□   on   0.118
——— off   0
– – – on   0

Tails   k

○   off   0.113
□   on   0.113
——— off   0
– – – on   0

$C_{m_\alpha} - k^2 C_{m_q}$

$C_{A_\alpha} - k^2 C_{A_q}$

$C_{N_\alpha} - k^2 C_{N_q}$

α, deg

Heat shield 4 (reentry configuration)

Heat shield 1 (landing configuration)
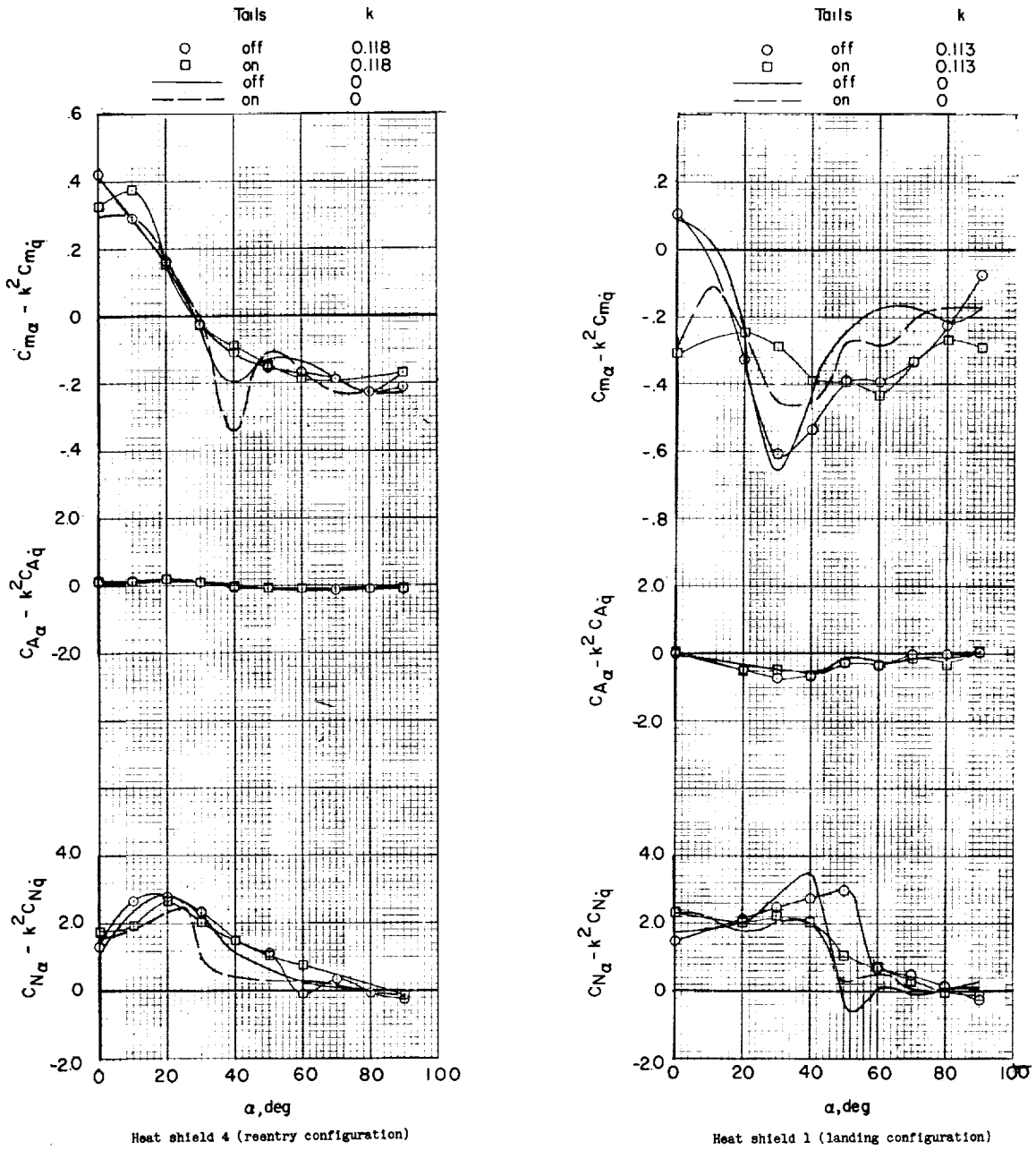
(a) In-phase derivatives.

Figure 10.- Pitching oscillatory derivatives measured in forced oscillation tests in pitch.

Heat shield 4 (reentry configuration)

Heat shield 1 (landing configuration)
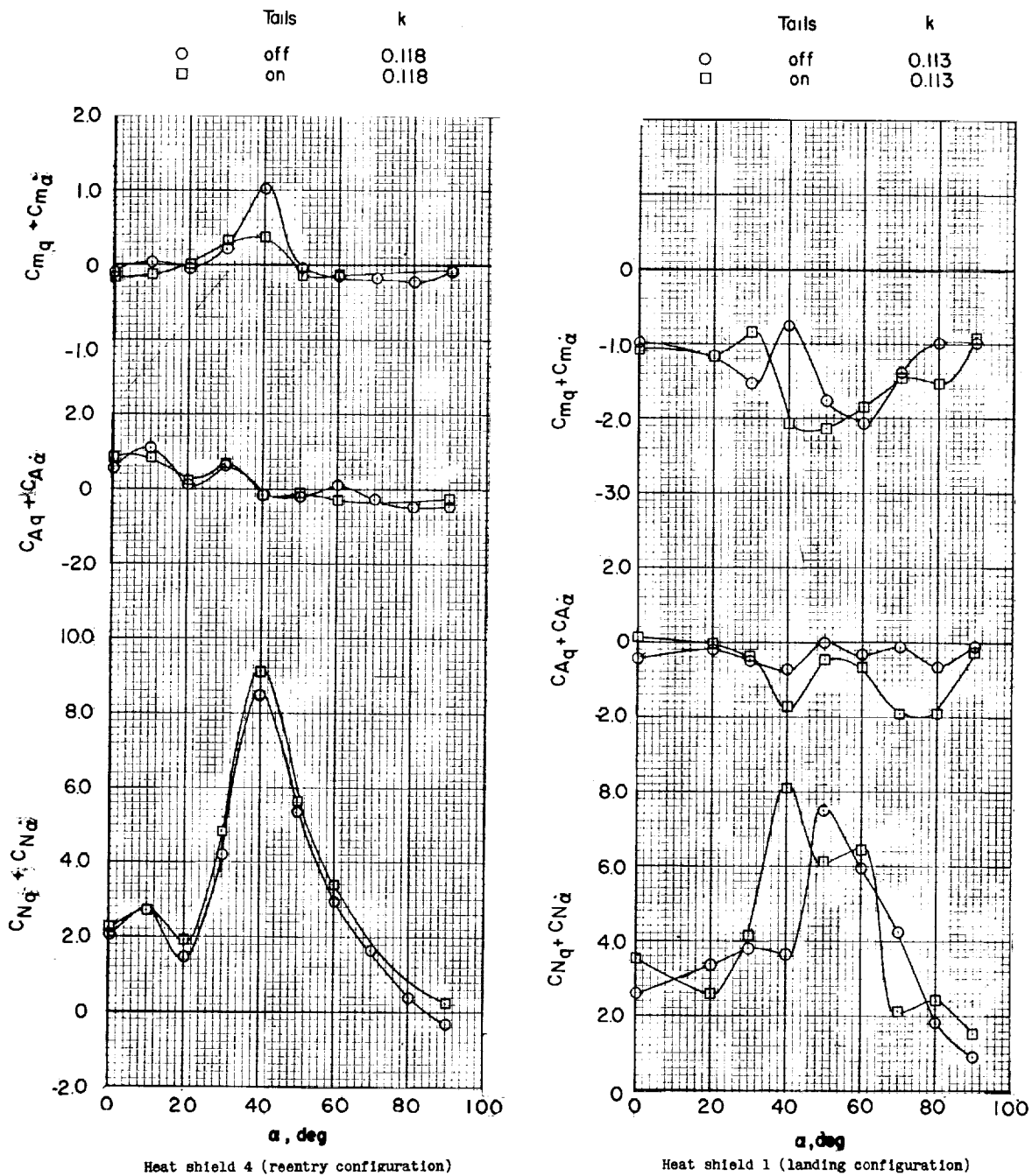
(b) Out-of-phase derivatives.

Figure 10.- Concluded.
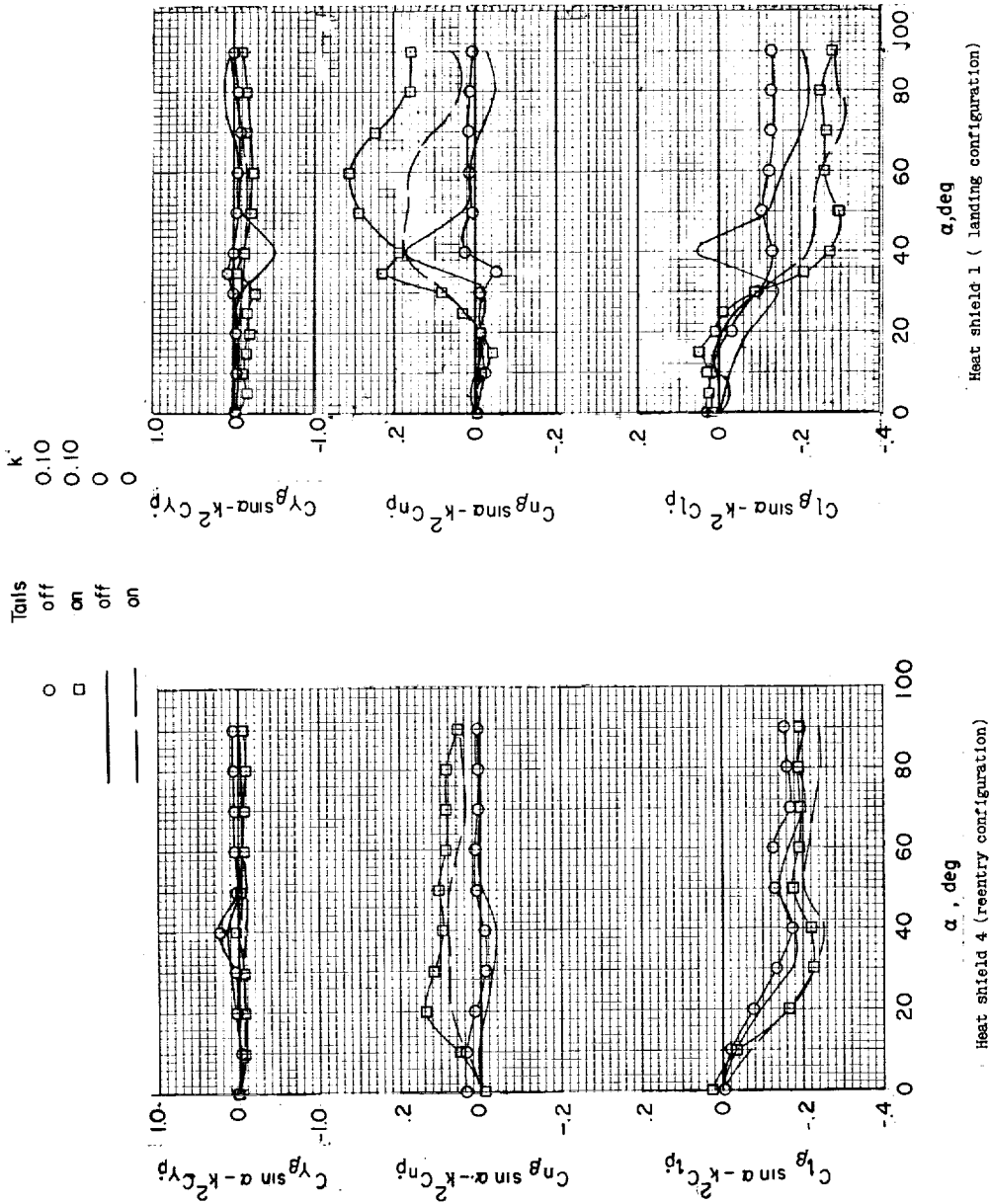
(a) Rolling oscillation derivatives.

Figure 11.- In-phase lateral oscillatory derivatives measured in forced oscillation tests in roll and yaw.

L-1329

Heat shield 4 (reentry configuration)

Heat shield 1 (landing configuration)
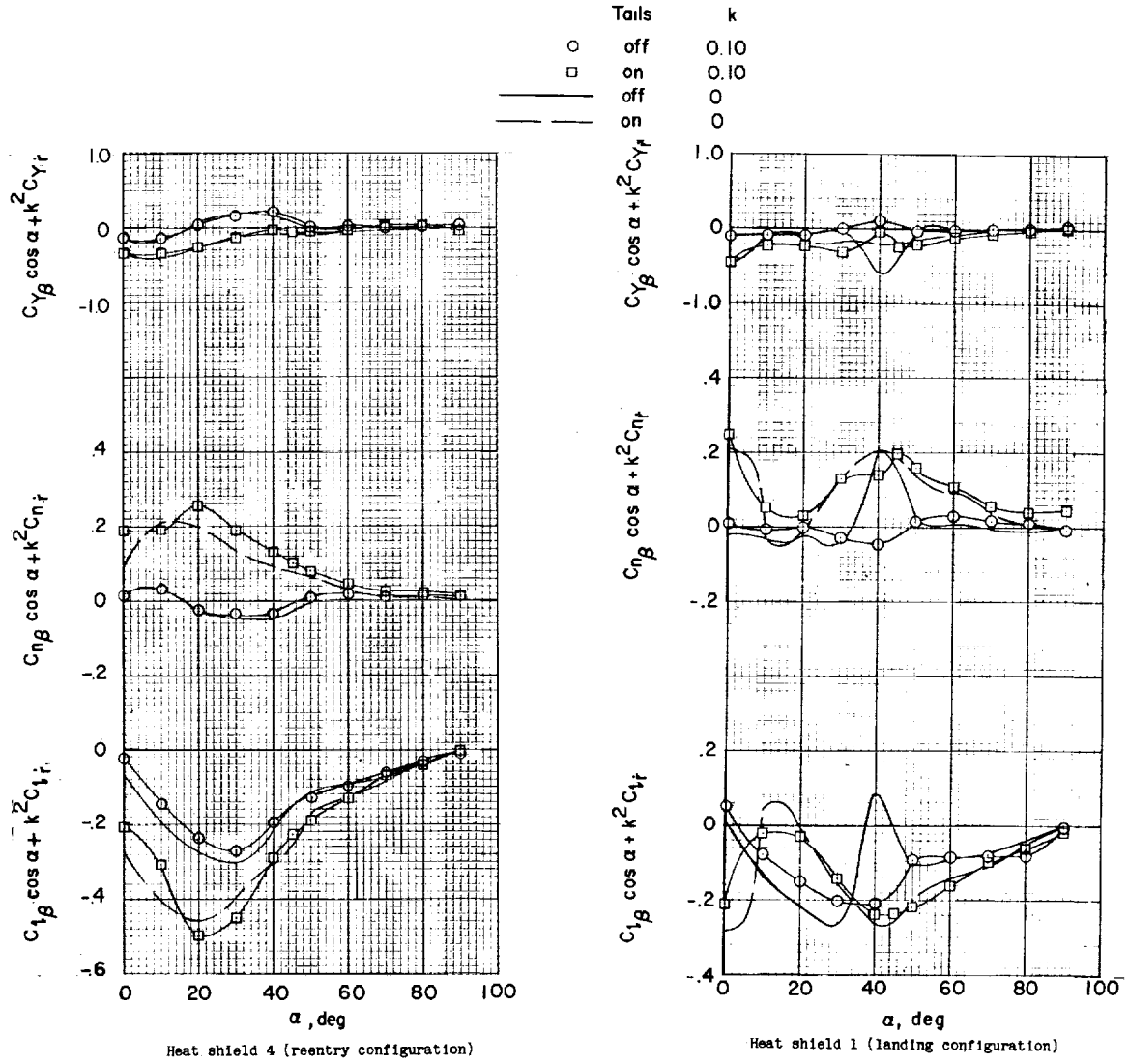
(b) Yawing oscillation derivatives.

Figure 11.- Concluded.
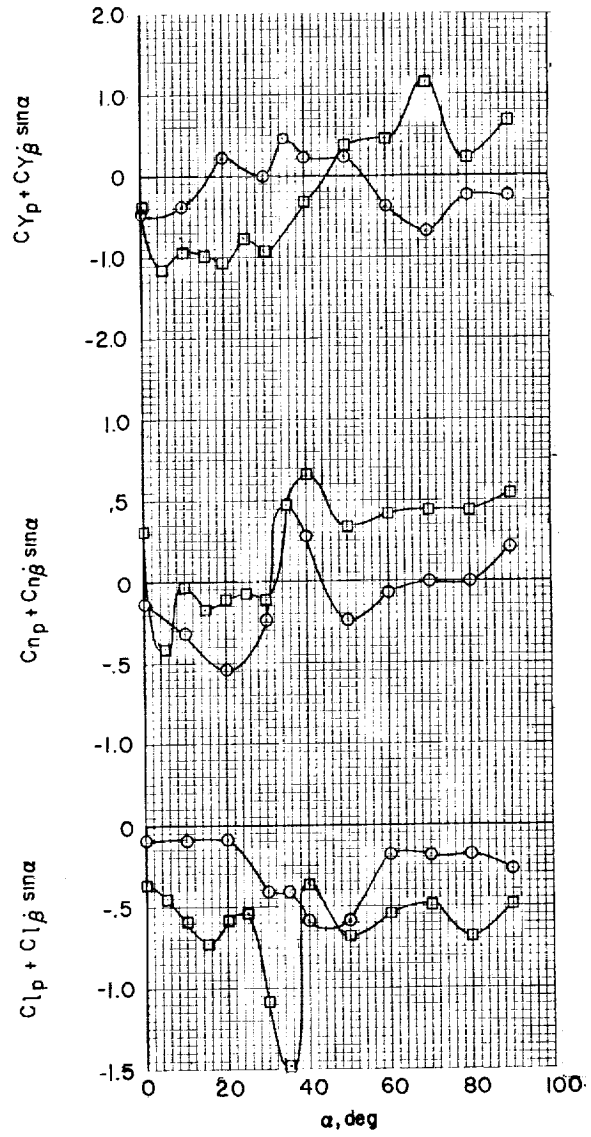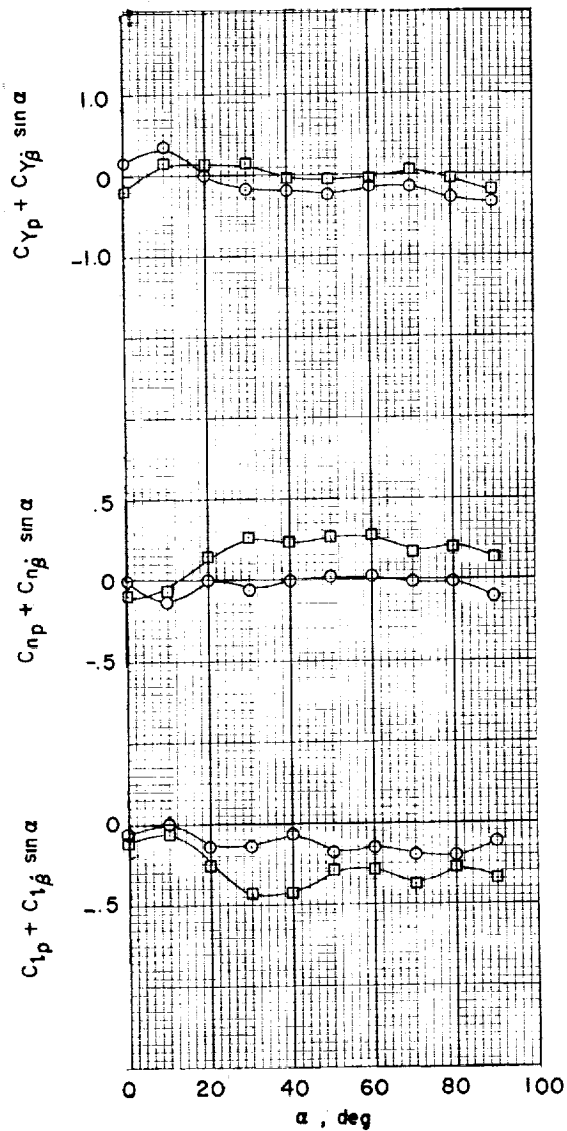
Figure 12.- Out-of-phase rolling oscillatory derivatives measured in forced oscillation tests in roll.
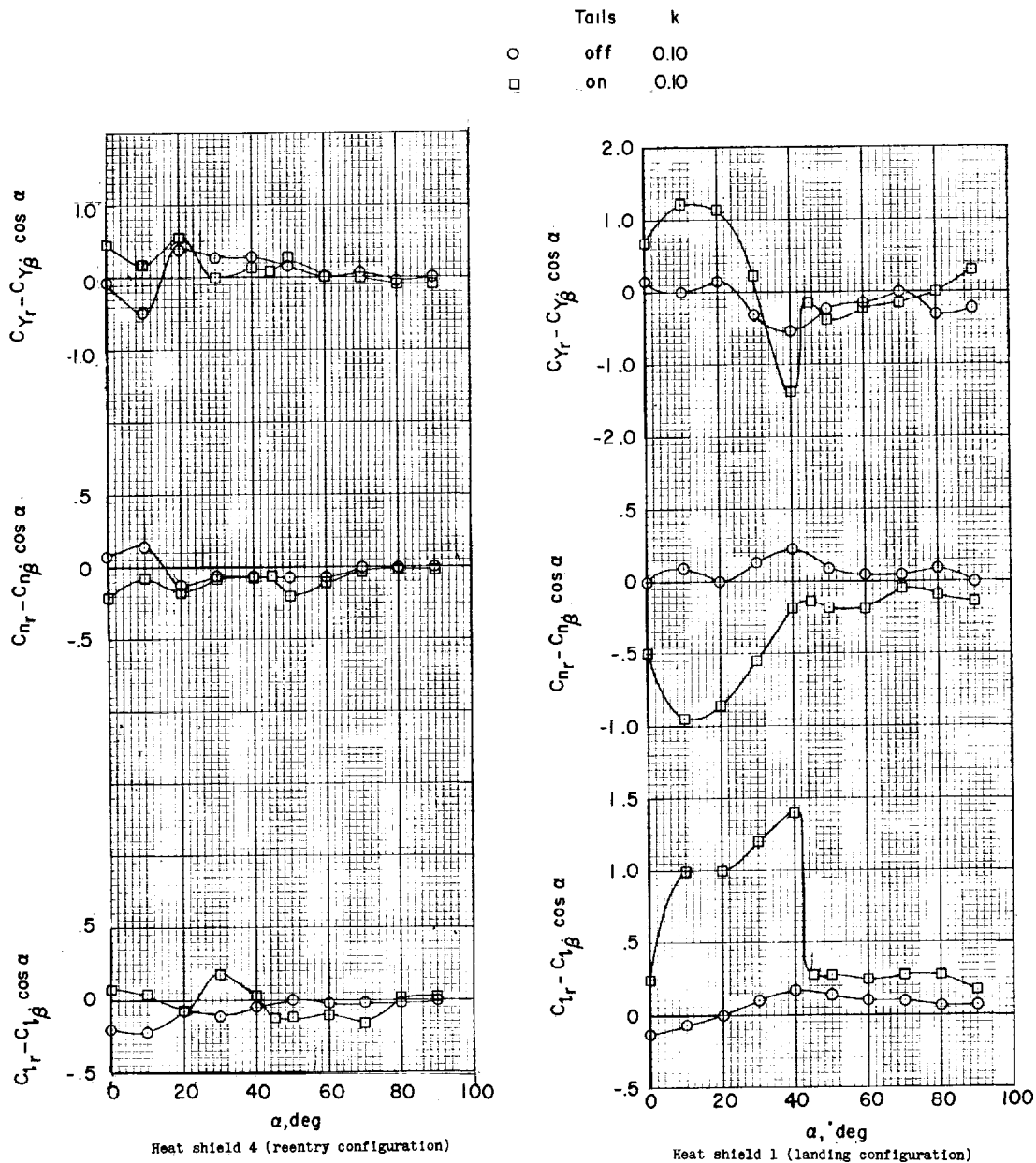
Figure 13.- Out-of-phase yawing oscillatory derivatives measured in forced oscillation tests in yaw.